All-Optical Switching and Unidirectional Plasmon Launching with Nonlinear Dielectric Nanoantennas

Alex Krasnok, Sergey Li, Sergey Lepeshov, Roman Savelev, Denis G. Baranov, and Andrea Alú

Phys. Rev. Applied **9**, 014015 — Published 16 January 2018

DOI: 10.1103/PhysRevApplied.9.014015

All-Optical Switching and Unidirectional Plasmon Launching with Nonlinear Dielectric Nanoantennas

Alex Krasnok,[1,2,*] Sergey Li,[2] Sergey Lepeshov,[2] Roman Savelev,[2] Denis G. Baranov,[3,4] and Andrea Alú[1,*]
[1] *The University of Texas at Austin, Austin, Texas 78712, USA*
[2] *Laboratory of Nanophotonics and Metamaterials, ITMO University, St. Petersburg, Russia*
[3] *Department of Physics, Chalmers University of Technology, 412 96 Gothenburg, Sweden*
[4] *Moscow Institute of Physics and Technology, Dolgoprudny 141700, Russia*
[*] *E-mail: akrasnok@utexas.edu, alu@mail.utexas.edu*

High-index dielectric nanoparticles have become a powerful platform for nonlinear nanophotonics due to special types of optical nonlinearity like electron-hole plasma (EHP) photoexcitation. In this paper, a novel highly tunable dielectric nanoantenna consisting of a chain of silicon particles excited by a dipole emitter is proposed. The nanoantenna exhibits slow group velocity guided modes corresponding to the Van Hove singularity in an infinite structure, which enable a large Purcell factor up to several hundred and are very sensitive to the nanoparticles permittivity. This sensitivity enables the nanoantenna tuning via EHP excitation with an ultrafast laser pumping. Dramatic variations in the nanoantenna radiation patterns and Purcell factor caused by ultrafast laser pumping of several boundary nanoparticles with relatively low intensities of about 25 GW/cm^2 are shown. Unidirectional surface plasmon-polaritons launching with EHP excitation in the nanoantenna on an Ag substrate is demonstrated.

I. INTRODUCTION

In the last several years dielectric nanoparticles and nanostructures made of materials with large positive dielectric permittivity, such as Si, GaP, GaAs, have proved to be a promising platform for various nanophotonic applications [1–3]. The examples include functional nanoantennas [4–6], enhanced spontaneous emission [7–11], photovoltaics [12], frequency conversion [13–16], Raman scattering [17], and sensing [7, 18]. The great interest in such nanostructures is caused mainly by their ability to control the electric and magnetic components of light at the nanoscale as well as low dissipative loses and thermal heating [18]. In particular, it has been demonstrated that dielectric nanoantennas allow directional scattering of an incident light and effective transformation of the near field of feeding quantum emitters (QEs) into propagating electromagnetic waves [3, 7].

Modification of the spontaneous emission rate of a QE induced by its environment, known as the Purcell effect [19, 20], is not so pronounced for single dielectric nanoparticles [3, 21] in contrast to microcavities [22] and plasmonic nanoantennas [23, 24]. This is because of their relatively low quality factors and large mode volumes, which results in low efficiency of light-matter interaction. However, it was recently shown that this obstacle can be overcome by relying on slowly guided modes in chain nanostructures. It turned out that the Purcell factor can be increased by several orders of magnitude in finite chains of Si nanoparticles [25]. The role of Van Hove singularities associated with infinite structures in the high Purcell factor enhancement has been revealed by using an eigenmode analysis. Moreover, the collective nature of these modes makes the structure very sensitive to any changes in geometry opening the way to creation highly tunable devices.

High-index dielectric nanostructures are of a special interest for nonlinear nanophotonics because of their strong nonlinear response. It was recently predicted and experimentally demonstrated that photoexcitation of dense electron-hole plasma (EHP) in single Si nanoparticles [26–28] and Si nanodimers [29] by femtosecond laser (fs-laser) pulses is accompanied by a radiation properties modification, whereas generation of EHP in Ge nanoantennas can even turn them into plasmonic ones in the mid-IR region [30]. In this regard, we note that in contrast to metals, whose conduction band is already partially filled at room temperature, the conduction band of semiconductors is almost empty and generation of EHP

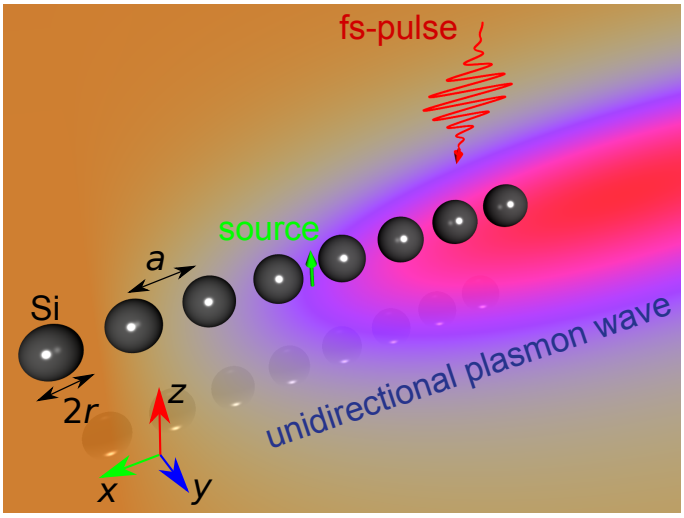

FIG. 1. Schematic presentation of the nonlinear dielectric nanoantenna tunable with electron-hole plasma photoexcitation via fs-laser pulse pumping of a few boundary nanoparticles. Nanoantenna allows tuning the Purcell factor and radiation power pattern of a QE (green arrow), and enables unidirectional launching of propagating plasmonic surface waves.

may significantly modify their plasma frequency and dielectric permittivity [28].

Here, we combine the concepts of Van Hove singularity and EHP excitation together and propose a highly tunable dielectric nanoantenna, consisting of a Si nanoparticles chain excited by an electric dipole emitter. The nanoantenna possess slowly guided modes corresponding to the Van Hove singularity in an infinite chain. Since these modes are very sensitive to the nanoparticle permittivity, the radiation properties of nanoantenna become extremely sensitive to EHP photoexcitation. We theoretically and numerically demonstrate the tuning of radiation power patterns and Purcell factor by pumping several boundary nanoparticles in the chain with relatively low peak intensities of fs-laser pulses. Moreover, we show that the proposed nanoantenna, being excited by fs-laser pulses, allows unidirectional launching of surface plasmon-polariton (SPP) waves (Fig. 1), making this solution attractive for all-optical light manipulation systems. We note that in contrast to the established approaches to unidirectional SPP waves excitation [31–35], nonlinear waveguiding systems with QEs as a source are still weakly developed, while they may have many important applications in nanophotonics and quantum optics.

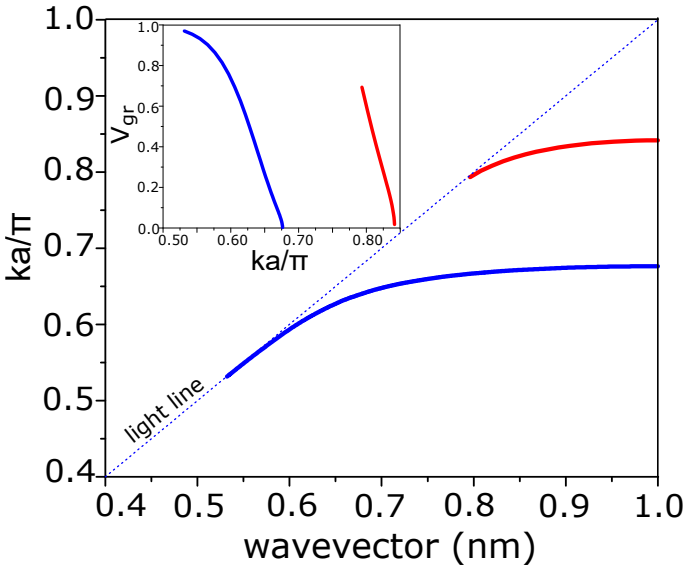

FIG. 2. Dispersion diagram of an infinite chain of dielectric nanoparticles with radius $r = 70$ nm and period $a = 200$ nm. Inset: group velocity (V_{gr}) of waveguiding modes in the infinite chain as a function of normalized frequency. The blue and red curves correspond to TM- and TE-modes, respectively.

II. RESULTS AND DISCUSSION

To briefly recall the origin of the *Van Hove singularity*, let us consider a generic periodic one-dimensional system supporting a set of guided modes. Decomposing its Green tensor into a series of eigenmodes, one can calculate the Purcell factor in such a system according to Ref. [36]

$$F \simeq \frac{1}{\pi}\left(\frac{\lambda}{2}\right)^2 \frac{c}{A_{\text{eff}} V_{\text{gr}}}, \tag{1}$$

with A_{eff} being the effective area of the resonant guided mode, λ the free space wavelength, V_{gr} the group velocity of the mode, and c is the speed of light. The divergence of the Purcell factor, occurring at the point of zero group velocity, is known as a Van Hove singularity. This expression clearly suggests that the Purcell factor benefits from slow light modes of the structure. In reality, its finite size prevents this divergence, but nevertheless largely enhanced Purcell factor can still be traced to the Van Hove singularity of the original structure, as has been theoretically and experimentally shown in Ref. [25].

Here, we realize a Van Hove singularity using a chain of N spherical dielectric nanoparticles excited by an electric dipole (green arrow), placed in the center of chain and perpendicularly oriented to the chain axis, Fig. 1. We choose Si particles with dielectric permittivity ε_1 close to 16 in the operational frequency range [37]. The nanoparticles have all the same radius r and the center-to-center distance between neighboring particles is a.

The optical properties of nanoparticle-based nanoantennas can be understood from the infinite chain modal dispersion [38, 39]. Therefore we start by calculating the optical properties of the infinite structure with an analytical approach, based on the well-known coupled-dipole model. Each particle is modeled as a combination of magnetic and electric dipoles with magnetic $\mathbf{m}$ and electric $\mathbf{p}$ momenta, oscillating with frequency ω [$\propto \exp(-i\omega t)$]. In the CGS system this approach leads to the linear system of equations:

$$\begin{aligned} \mathbf{p}_i &= \alpha_{ei} \sum_{j\neq i} \left(\widehat{C}_{ij}\mathbf{p}_j - \widehat{G}_{ij}\mathbf{m}_j \right), \\ \mathbf{m}_i &= \alpha_{mi} \sum_{j\neq i} \left(\widehat{C}_{ij}\mathbf{m}_j + \widehat{G}_{ij}\mathbf{p}_j \right), \end{aligned} \tag{2}$$

where $\widehat{C}_{ij} = A_{ij}\widehat{I} + B_{ij}(\hat{\mathbf{r}}_{ij} \otimes \hat{\mathbf{r}}_{ij})$, $\widehat{G}_{ij} = -D_{ij}\hat{\mathbf{r}}_{ij} \times \widehat{I}$, $\otimes$ is the dyadic product, $\widehat{I}$ is the unit 3×3 tensor, $\hat{\mathbf{r}}_{ij}$ is the unit vector in the direction from i-th to j-th sphere, and

$$\begin{aligned} A_{ij} &= \frac{\exp(ik_h r_{ij})}{r_{ij}} \left(k_h^2 - \frac{1}{r_{ij}^2} + \frac{ik_h}{r_{ij}} \right), \\ B_{ij} &= \frac{\exp(ik_h r_{ij})}{r_{ij}} \left(-k_h^2 + \frac{3}{r_{ij}^2} - \frac{3ik_h}{r_{ij}} \right), \\ D_{ij} &= \frac{\exp(ik_h r_{ij})}{r_{ij}} \left(k_h^2 + \frac{ik_h}{r_{ij}} \right), \end{aligned} \tag{3}$$

where r_{ij} is the distance between the centers of i-th and j-th spheres, ε_h is the permittivity of the host medium, $k_h = \sqrt{\varepsilon_h}\omega/c$ is the host wavenumber, $\omega = 2\pi\nu$, and ν is the frequency. The quantities α_m and α_e are the magnetic and electric polarizabilities of a spherical par-

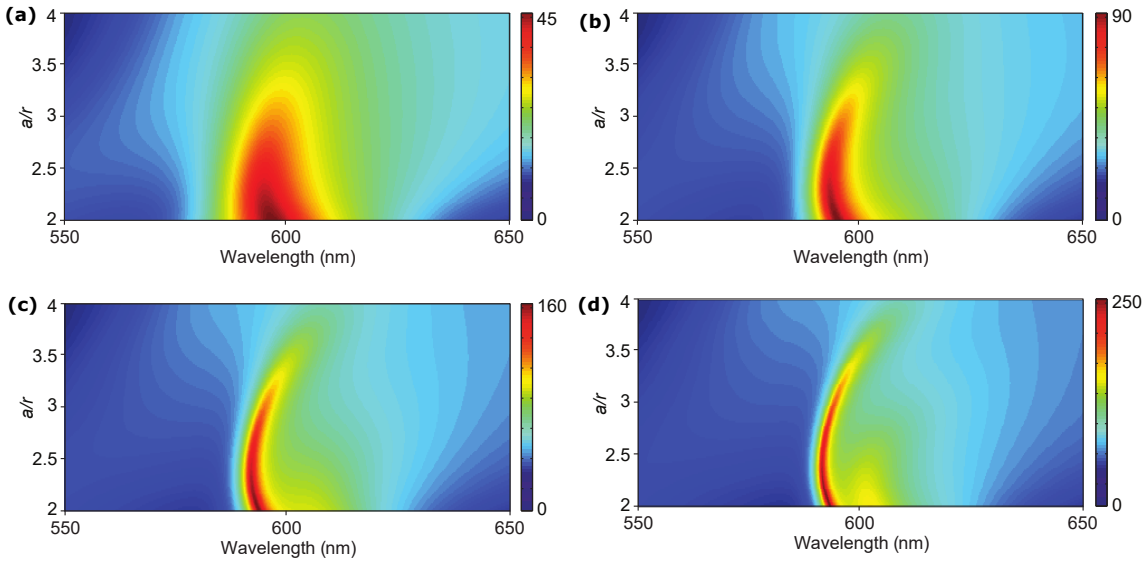

FIG. 3. Log-scale Purcell factor as the function of the radiation wavelength and ratio r/a for the dielectric chain with $\varepsilon_1 = 16$, for different number of nanoparticles: (a) $N = 4$, (b) $N = 6$, (c) $N = 8$, and (d) $N = 10$; r is taken equal to 70 nm, a is a period of the chain.

ticle [40]:

$$\alpha_e = i\frac{3\varepsilon_h a_1}{2k_h^3}, \quad \alpha_m = i\frac{3b_1}{2k_h^3}, \tag{4}$$

where a_1 and b_1 are electric and magnetic Mie coefficients. The coupled dipole approximation outlined above is justified for the geometrical parameters of the nanoparticles and their relative distance [41].

The solution of Eq. 2 without source [dispersion of waveguide eigenmodes $\omega(k)$] for the infinite dielectric chain with $r = 70$ nm and $a = 200$ nm in free space is shown in Fig. 2. Here, we use the dimensionless wavenumber $q = \beta a/\pi$, where β is the Bloch propagation constant. For simplicity but without loss of generality we model silicon by a material with permittivity of 16 at the wavelength of 600 nm, which is close to experimental data [37]. The blue and red curves correspond to transverse magnetic (TM) and transverse electric (TE) modes, respectively, which are the only modes excited by the dipole QE with the chosen orientation. Both of these modes are characterized by induced magnetic and electric moments (except the points at the band edge). Due to the spectral separation of resonances of the single particle, the magnetic moments are dominant in the first branch (TM), and electric moments in the second one (TE). The inset in Fig. 2 shows the calculated group velocities of the waveguide modes as a function of frequency. It can be seen that the group velocity $V_{\rm gr}$ drops to zero at the band edge around $ka/\pi \approx 0.675$ and $ka/\pi \approx 0.83$. Since the symmetry of the ED source matches the symmetry of the TM staggered mode (and not the TE one), we may expect significant enhancement of the Purcell factor for a finite system around the first frequency.

To confirm this expectation, we calculate the Purcell factor using the Green's tensor approach [42]:

$$F = \frac{3}{2k_h^3}\mathbf{z}\cdot \mathrm{Im}[\mathbf{G}\,(0,0;\omega)]\cdot\mathbf{z} \tag{5}$$

with $\mathbf{G}\,(0,0;\omega)$ being Green's tensor of an electric dipole in the center of chain (point of the dipole QE localization) and $\mathbf{z}$ being the unit vector pointing in the z direction (Fig. 1). Practically, the quantity $\mathrm{Im}[\mathbf{G}\,(0,0;\omega)]$ can be found by solving the scattering problem with a dipolar QE outlined above, Eqs. (2)–(4).

Fig. 3 shows the calculated Purcell factor as a function of wavelength and ratio r/a for a QE located in the center of a dielectric chain with different number of particles: (a) $N = 4$, (b) $N = 6$, (c) $N = 8$, and (d) $N = 10$. We observe that increasing the number of nanoparticles N gives rise to enhancement of Purcell factor. For example, the maximal value of the Purcell factor for $N = 10$ reaches 250. Along with the calculations shown in Fig. 2, we conclude that the maximum of Purcell factor arises around the Van Hove singularity.

Now, we are ready to show that the excitation of slow guided modes determining a Van Hove singularity is very sensitive to the electrodynamic properties of the system. Our aim is to utilize this effect to engineer highly tunable nanoantennas, for which relatively low intensities of external laser pulses can control and cause a dramatic modification of the optical properties of the material, and consequently the radiation properties (intensities of emission and power patterns) of the nanoantenna. To enable the switching of the nanoantenna properties we employ the nonlinear response caused by *electron-hole plasma photoexcitation* the in boundary particles of the Si nanoantenna.

To describe EHP-induced tuning of the nanoantenna, we employ the analytical approach developed in Ref. [28]. The dynamics of volume-averaged EHP density $\rho_{\rm eh}$ is modeled via the rate equation

$$\frac{d\rho_{\rm eh}}{dt} = -\Gamma\rho_{\rm eh} + \frac{W_1}{\hbar\omega} + \frac{W_2}{2\hbar\omega}, \qquad (6)$$

where, $W_{1,2}$ are the volume-averaged absorption rates due to one- and two-photon processes, and Γ is the EHP recombination rate which depends on EHP density [43]. The absorption rates are written in the usual form as $W_1 = \frac{\omega}{8\pi}\left\langle\left|\tilde{\mathbf{E}}_{\rm in}\right|^2\right\rangle {\rm Im}(\varepsilon)$ and $W_2 = \frac{\omega}{8\pi}\left\langle\left|\tilde{\mathbf{E}}_{\rm in}\right|^4\right\rangle {\rm Im}\,\chi^{(3)}$, where angle brackets denote averaging over the nanoparticle volume, and ${\rm Im}\,\chi^{(3)} = \frac{\varepsilon c^2}{8\pi\omega}\beta_{\rm TPA}$ with $\beta_{\rm TPA}$ being two-photon absorption coefficient. The relaxation rate of EHP in c-Si is dominated by Auger recombination $\Gamma = \Gamma_{\rm A}\rho_{\rm eh}^2$ with $\Gamma_{\rm A} = 4\cdot 10^{-31}$ s^{-1}cm^6 (Ref. [44]).

Eq. 6 describes the volume averaged concentration of EHP $\rho_{\rm eh}$(t) neglecting its spatial distribution and hence diffusion of carriers across the particle volume. At $\rho_{\rm eh} > 10^{20}$ cm^{-3} the thermal velocity of hot free electrons is about $v \approx 5\times 10^5$ cm/s [45], whereas the corresponding electron-electron scattering time is about ∼100 fs. The characteristic EHP homogenization time governed by a ballistic motion of electrons therefore can be estimated as $\tau_{\rm hom} \approx r/2v \approx 100$ fs, where r is the nanoparticles radius. As one can see, the estimated diffusion time is much smaller than the EHP recombination time and is comparable to the incident pulse duration.

The permittivity of photoexcited Si should be related to time-dependent EHP density:

$$\varepsilon(\omega,\rho_{\rm eh}) = \varepsilon_0 + \Delta\varepsilon_{\rm bgr} + \Delta\varepsilon_{\rm bf} + \Delta\varepsilon_{\rm D}, \qquad (7)$$

where ε_0 is the permittivity of non-excited material, while $\Delta\varepsilon_{\rm bgr}$, $\Delta\varepsilon_{\rm bf}$, and $\Delta\varepsilon_{\rm D}$ are the contributions from bandgap renormalization, band filling, and Drude term, respectively. The detailed expressions for all contributions in Eq. (7) can be found in Ref. [28]. In total, these three contributions lead to decrease of the real part of permittivity with increasing EHP density.

The spectral dependency of the Purcell factor before and after EHP photoexcitation are presented in Fig. 4 for the different number of particles N. The calculations are performed for the change of real part of Si permittivity $\Delta\varepsilon = -1$ [where $\Delta\varepsilon = \varepsilon(\omega,\rho_{\rm eh}) - \varepsilon_0$], which is achieved at the wavelength of 600 nm upon excitation of the EHP with density $\rho_{eh} \approx 10^{21}$ cm^{-3}. The decrease of Purcell factor approximately by a factor of 2 in all cases, Figs. 4(a),(c),(e), along with the spectral broadening are caused by symmetry breaking of the chain and corresponding decrease of the quality factor of the Van Hove singularity mode. The EHP photoexcitation also modifies the radiation pattern of the nanoantenna, Figs. 4(b),(d),(f). Before the plasma excitation ($\Delta\varepsilon = 0$) the radiation pattern exhibits two symmetric lobes directed along the chain axis in forward and backward directions (red curves). In this case, the maximal value of

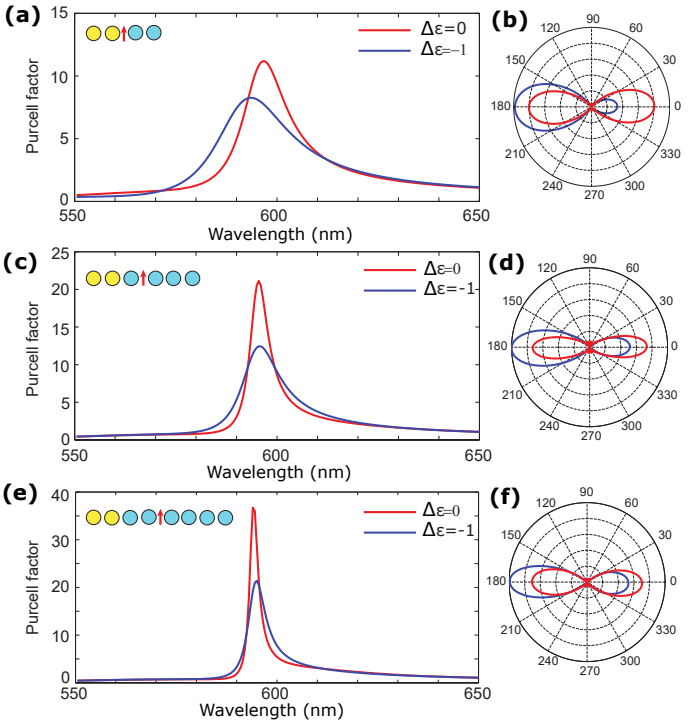

FIG. 4. (a),(c),(e) Spectral dependence of the Purcell factor for the chains of dielectric nanoparticles ($r = 70$ nm) for different number of nanoparticles N: (a) $N = 4$; (c) $N = 6$; (e) $N = 8$. (b),(d),(f) Radiation power patterns (E-plane) of the QE at the radiation wavelength of 600 nm for different number of nanoparticles N. Red curves correspond to the unaffected chains ($\Delta\varepsilon = 0$), whereas the blue ones correspond to the chains with photo-excited boundary particles ($\Delta\varepsilon = -1$).

directivity grows with increasing of N. After the plasma excitation ($\Delta\varepsilon = -1$), the nanoantenna radiates mostly in the direction of affected particles. We note that the degree of modification of the radiation pattern grows with increasing number of particles. For example, in the case of $N = 8$ [Fig. 4(f)], the directivity in left direction is almost two times larger that in the right one. Thus, the EHP photoexcitation can be applied for all-optical switching of radiation patterns. Such dramatic tuning of the radiation pattern is caused by the Van Hove singularity regime of the initially unaffected nanoantenna. We notice that the proposed nanoantenna exhibits the QE position tolerance of about 30 nm [46], which is enough for practical realization with existing technologies of QDs positioning [47].

In the vast majority of nanoantenna realizations, the substrate substantially affects the nanoantenna characteristics (see, for example, Ref. [48]). For this reason, we analyze how a SiO_2 substrate affects the nanoantenna's characteristics. To simulate the nanoantenna consisting of 8 nanoparticles, located on the SiO_2 substrate with $\varepsilon_{\rm sub} = 2.21$, we utilize the commercial software CST Microwave Studio. To calculate the Purcell factor, the method based on the input impedance of a small (in

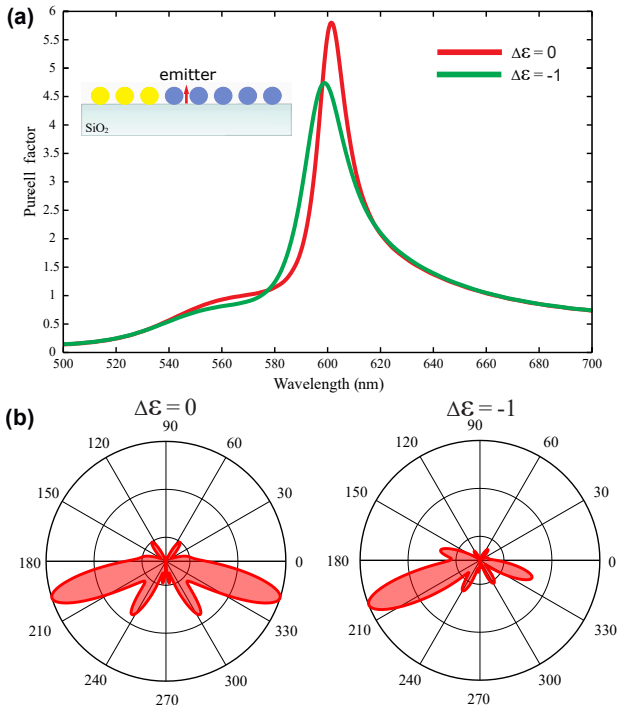

FIG. 5. (a) Purcell factor for the chain of $N = 8$ Si spherical particles ($r = 70$ nm) arranged on a SiO_2 substrate as a function of radiation wavelength. Differences of the dielectric permittivity of unaffected and three left boundary affected particles are $\Delta\varepsilon = 0$ (red curve) and $\Delta\varepsilon = -1$ (green curve). (b) Power patterns for different $\Delta\varepsilon$.

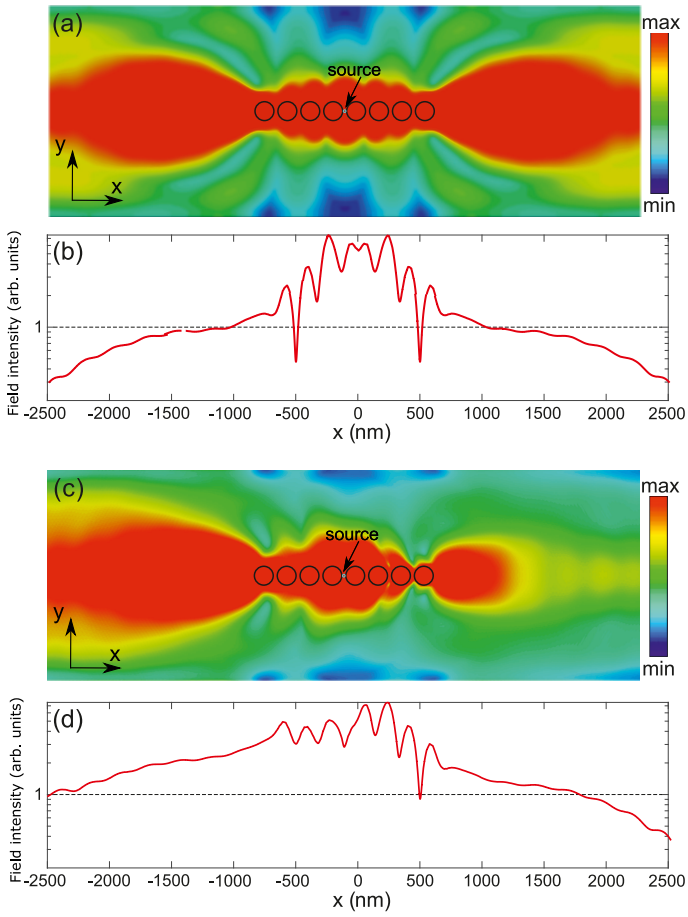

FIG. 6. Radiation of the nanoantenna composed by 8 Si spherical particles ($r = 70$ nm) placed with the period of 200 nm on a Ag substrate with the 60 nm spacer glass layer; QE is located at the center of the chain perpendicularly to the substrate. (a,c) Electric field distribution profiles in the plane orthogonal to the QE in the cases of unaffected $\Delta\varepsilon = 0$ and affected $\Delta\varepsilon = -1$ three left boundary nanoparticles, respectively. (b,d) Electric field intensities as a function of x coordinate in the cases of unaffected and affected three boundary nanoparticles, respectively. Emission wavelength is 600 nm.

terms of radiation wavelength) dipole antenna [49] has been applied. The corresponding results are presented in Fig. 5(a). These spectra qualitatively agree with our analytical calculations presented above. However, in this case, the substrate breaks the mirror symmetry with respect to the z axis, which leads to a reduction of Purcell factor. From the experimental standpoint, a laser pulse can be tightly focused to a sub-wavelength spot by an oil immersion microscope objective with a large numerical aperture (NA). For example, an objective with NA=1.4 can provide the full-width at half-maximum diameter of the beam focal spot size of d=560 nm at the wavelength of 650 nm according to the relation $d \approx 1.22\lambda/NA$ [50, 51]. This spot size correspond to three boundary nanoparticles that should be assumed to be affected [see inset in the Fig. 5(a)]. During the EHP photoexcitation, the maximum of Purcell factor slightly decreases from 5.9 to 4.7 accompanied by shifting of the resonant frequency to the shorter wavelengths due to the decrease of boundary particles dielectric permittivity.

Fig. 5(b) demonstrates the change in radiation pattern induced by EHP photoexcitation for the nanoantenna on SiO_2 substrate. When $\Delta\varepsilon$=0 (unaffected nanoantenna) the radiation power pattern is symmetric with respect to the dipole axis and has two main lobes. It can be observed that the mirror symmetry of the radiation patterns with respect to the z axis is broken, and the main lobes are oriented into the substrate, which has higher refractive index than the upper space. The modification of three boundary particles dramatically changes the power pattern: the reconfiguration is sufficient for practical applications even for $\Delta\varepsilon = -1$.

This effect can be used for the unidirectional launching of waveguide modes in plasmonic waveguides at will. Fig. 6 demonstrates this phenomenon, showing the calculated radiation of a nanoantenna composed of 8 Si nanoparticles placed with the period of 200 nm on a silver substrate with the 60 nm spacer glass (SiO_2) layer. The SiO_2 spacer serves as a buffer layer for the protection of silver substrate from sulfidation. The QE is located at the center of chain perpendicular to the substrate. Figs. 6(a) and (b) show the electric field distribution profile and the electric field intensity as a function of the x

coordinate in the cases of the unaffected nanoantenna, respectively. It can be seen that the nanoantenna launches surface plasmons symmetrically to the positive and negative directions of axis x. However, when three boundary nanoparticles are illuminated by the pump beam, the nanoantenna launches surface plasmons almost unidirectionally, Figs. 6(c,d). We achieve a value of front-to-back ratio up to 5 for this geometry, Fig. 6(d). The plots in Figs. 6(b),(c) exhibit two types of oscillations: in vicinity of the nanoantenna and aside from it. The first one is caused by field localization around Si nanoparticles due to their resonant response. The second one is due to a small reflection from open boundaries in the simulation region. This reflection is caused by the Ag substrate with real loses and dispersion.

We note that the methods to create the proposed nanoantenna do exist. Namely, in Ref. [52] the method to assemble colloidal nanoparticles of different nature (dielectric, metallic, polymeric) has been proposed. It has been demonstrated that structures of any complexity and composition can be created from sub-500 nm nanoparticles under a light- controlled temperature field. We believe that this approach can be applied directly for our nanoantenna fabrication. We note that the proposed approach to the nonlinear nanoantenna design also works for nanoantennas composed of cylindrical nanoparticles [53], which can be fabricated by existing lithography-based methods.

As a next step of our analysis, we estimate the parameters of a pump pulse required for generation of 10^{21} cm^{-3} EHP, assumed in the electromagnetic calculations above. At the high intensities required for photoexcitation of Si, two-photon absorption (TPA) usually dominates over one-photon process [28]. Silicon has a particularly large TPA coefficient between 600 and 700 nm [54]. We set the wavelength of pump pulse to 650 nm in order to avoid the interference between pump and QE signals. Estimating the enhancement factors for $\left\langle \left|\tilde{\mathbf{E}}_{\text{in}}\right|^2 \right\rangle$ and $\left\langle \left|\tilde{\mathbf{E}}_{\text{in}}\right|^4 \right\rangle$ for a Si nanoparticle on a substrate and using equations (6) to calculate the dynamics of EHP density, we find that a 200 fs pulse with peak intensity of 25 GW/cm^2 provides 10^{21} cm^{-3} EHP in the nanoparticle on a silver substrate. The EHP relaxation time at such density is about 2-3 ps as has been reported in Refs. [28, 29] that should be sufficient for ultrafast modulation of the emission process of a typical emitter with lifetime lying in the nanosecond range.

Finally, we stress that the intensity of ∼25 GW/cm^2 is much weaker than typical values of damage threshold for metallic and dielectric nanostructures. For example, gold nanorods have the damage threshold of ∼70 GW/cm^2 or ∼10 mJ/cm^2 at 130 fs [55], gold G-shaped nanostructures: ∼100 GW/cm^2 or ∼3 mJ/cm^2 at 30 fs [56], and gold nanocylinders: ∼200 GW/cm^2 or ∼20 mJ/cm^2 at 100 fs [57]. According to the known data from literature, low-loss silicon nanoparticles have significantly higher damage threshold: ∼400 GW/cm^2 or ∼100 mJ/cm^2 at 250 fs [58]; and ∼1000 GW/cm^2 or ∼100 mJ/cm^2 at 100 fs [26].

III. CONCLUSIONS

In conclusion, we have proposed the highly tunable all-dielectric nanoantenna, consisting of a chain of Si nanoparticles excited by a quantum emitter, that allow tuning their radiation properties via electron-hole plasma photoexcitation. We have theoretically and numerically demonstrated the tuning of radiation power patterns and the Purcell effect by additional pumping several boundary nanoparticles with relatively low peak intensities. We have also demonstrated that these effects remain valid for the nanoantenna situated on a dielectric surface. The proposed nanoantenna allows tunable unidirectional launching of surface plasmon waves, with interesting implications for modern nonlinear nanophotonics.

ACKNOWLEDGMENTS

This work was financially supported by Russian Science Foundation (Grant 15-19-30023) and by Russian Foundation for Basic Research (Project 16-37-60076). This work was also partially supported by the Air Force Office of Scientific Research.

[1] Arseniy I. Kuznetsov, Andrey E. Miroshnichenko, Mark L. Brongersma, Yuri S. Kivshar, and Boris Luk'yanchuk, Optically resonant dielectric nanostructures, Science **354**, aag2472 (2016).
[2] Saman Jahani and Zubin Jacob, All-dielectric metamaterials, Nature Nanotechnology **11**, 23–36 (2016).
[3] Alexander E Krasnok, Andrey E Miroshnichenko, Pavel A Belov, and Yuri S Kivshar, All-dielectric optical nanoantennas, Optics Express **20**, 20599–20604 (2012).
[4] Brice Rolly, Jean-Michel Geffrin, Redha Abdeddaim, Brian Stout, and Nicolas Bonod, Controllable emission of a dipolar source coupled with a magneto-dielectric resonant subwavelength scatterer, Scientific Reports (2013).
[5] Alexander E Krasnok, Constantin R Simovski, Pavel A Belov, and Yuri S Kivshar, Superdirective dielectric nanoantennas, Nanoscale **6**, 7354–7361 (2014).
[6] Sergey V Li, Denis G Baranov, Alexander E Krasnok, and Pavel A Belov, All-dielectric nanoantennas for unidirectional excitation of electromagnetic guided modes, Applied Physics Letters **107**, 171101 (2015).
[7] Alex Krasnok, Martin Caldarola, Nicolas Bonod, and Andrea Alú, Spectroscopy and Biosensing with Op-

tically Resonant Dielectric Nanostructures, **ArXiv: 1710.10233** (2017).

[8] Raju Regmi, Johann Berthelot, Pamina M. Winkler, Mathieu Mivelle, Julien Proust, Frédéric Bedu, Igor Ozerov, Thomas Begou, Julien Lumeau, Hervé Rigneault, María F. García-Parajó, Sébastien Bidault, Jérôme Wenger, and Nicolas Bonod, All-Dielectric Silicon Nanogap Antennas To Enhance the Fluorescence of Single Molecules, Nano Letters **16**, 5143–5151 (2016).

[9] Dorian Bouchet, Mathieu Mivelle, Julien Proust, Bruno Gallas, Igor Ozerov, Maria F. Garcia-Parajo, Angelo Gulinatti, Ivan Rech, Yannick De Wilde, Nicolas Bonod, Valentina Krachmalnicoff, and Sébastien Bidault, Enhancement and inhibition of spontaneous photon emission by resonant silicon nanoantennas, Phys. Rev. Applied **6**, 064016 (2016).

[10] S Sun, L Wu, P Bai, and CE Png, Fluorescence enhancement in visible light: dielectric or noble metal? Physical Chemistry Chemical Physics **18**, 19324–19335 (2016).

[11] Alexander E Krasnok, Alex Maloshtan, Dmitry N Chigrin, Yuri S Kivshar, and Pavel A Belov, Enhanced emission extraction and selective excitation of nv centers with all–dielectric nanoantennas, Laser & Photonics Reviews **9**, 385–391 (2015).

[12] Mark L Brongersma, Yi Cui, and Shanhui Fan, Light management for photovoltaics using high-index nanostructures, Nature Materials **13**, 451–460 (2014).

[13] Alexander Krasnok, Mykhailo Tymchenko, and Andrea Alù, Nonlinear metasurfaces: a paradigm shift in nonlinear optics, Materials Today (2017), 10.1016/j.mattod.2017.06.007, arXiv:1706.07563.

[14] L Carletti, A Locatelli, O Stepanenko, G Leo, and C De Angelis, Enhanced second-harmonic generation from magnetic resonance in algaas nanoantennas, Optics Express **23**, 26544–26550 (2015).

[15] SV Makarov, AN Tsypkin, TA Voytova, VA Milichko, IS Mukhin, AV Yulin, SE Putilin, MA Baranov, AE Krasnok, IA Morozov, *et al.*, Self-adjusted all-dielectric metasurfaces for deep ultraviolet femtosecond pulse generation, Nanoscale **8**, 17809–17814 (2016).

[16] Alexander S. Shorokhov, Elizaveta V. Melik-Gaykazyan, Daria A. Smirnova, Ben Hopkins, Katie E. Chong, Duk-Yong Choi, Maxim R. Shcherbakov, Andrey E. Miroshnichenko, Dragomir N. Neshev, Andrey A. Fedyanin, and Yuri S. Kivshar, Multifold Enhancement of Third-Harmonic Generation in Dielectric Nanoparticles Driven by Magnetic Fano Resonances, Nano Letters **16**, 4857–4861 (2016).

[17] Pavel A Dmitriev, Denis G Baranov, Valentin A Milichko, Sergey V Makarov, Ivan S Mukhin, Anton K Samusev, Alexander E Krasnok, Pavel A Belov, and Yuri S Kivshar, Resonant raman scattering from silicon nanoparticles enhanced by magnetic response, Nanoscale **8**, 9721–9726 (2016).

[18] Martín Caldarola, Pablo Albella, Emiliano Cortés, Mohsen Rahmani, Tyler Roschuk, Gustavo Grinblat, Rupert F Oulton, Andrea V Bragas, and Stefan A Maier, Non-plasmonic nanoantennas for surface enhanced spectroscopies with ultra-low heat conversion, Nature Communications **6**, 7915 (2015).

[19] E. M. Purcell, Phys. Rev **69**, 681 (1946).

[20] Matthew Pelton, Modified spontaneous emission in nanophotonic structures, Nature Photon. **9**, 427 (2015).

[21] Sergey I. Bozhevolnyi and Jacob B. Khurgin, Fundamental limitations in spontaneous emission rate of single-photon sources, Optica **3**, 1418 (2016).

[22] Kerry J. Vahala, Optical microcavities, Nature **424**, 839–846 (2003).

[23] Kasey J. Russell, Tsung-Li Liu, Shanying Cui, and Evelyn L. Hu, Large spontaneous emission enhancement in plasmonic nanocavities, Nature Photon. **6**, 459–462 (2012).

[24] Gleb M. Akselrod, Christos Argyropoulos, Thang B. Hoang, Cristian Ciraci, Chao Fang, Jiani Huang, David R. Smith, and Maiken H. Mikkelsen, Probing the mechanisms of large purcell enhancement in plasmonic nanoantennas, Nature Photon. **8**, 835–840 (2014).

[25] Alexander Krasnok, Stanislav Glybovski, Mihail Petrov, Sergey Makarov, Roman Savelev, Pavel Belov, Constantin Simovski, and Yuri Kivshar, Demonstration of the enhanced purcell factor in all-dielectric structures, Applied Physics Letters **108**, 211105 (2016).

[26] Sergey Makarov, Sergey Kudryashov, Ivan Mukhin, Alexey Mozharov, Valentin Milichko, Alexander Krasnok, and Pavel Belov, Tuning of magnetic optical response in a dielectric nanoparticle by ultrafast photoexcitation of dense electron–hole plasma, Nano Letters **15**, 6187–6192 (2015).

[27] Maxim R. Shcherbakov, Polina P. Vabishchevich, Alexander S. Shorokhov, Katie E. Chong, Duk-Yong Choi, Isabelle Staude, Andrey E. Miroshnichenko, Dragomir N. Neshev, Andrey A. Fedyanin, and Yuri S. Kivshar, Ultrafast All-Optical Switching with Magnetic Resonances in Nonlinear Dielectric Nanostructures, Nano Letters **15**, 6985 (2015).

[28] Denis G. Baranov, Sergey V. Makarov, Valentin A. Milichko, Sergey I. Kudryashov, Alexander E. Krasnok, and Pavel A. Belov, Nonlinear Transient Dynamics of Photoexcited Resonant Silicon Nanostructures, ACS Photonics **3**, 1546–1551 (2016).

[29] Denis G Baranov, Sergey V Makarov, Alexander E Krasnok, Pavel A Belov, and Andrea Alù, Tuning of near-and far-field properties of all-dielectric dimer nanoantennas via ultrafast electron-hole plasma photoexcitation, Laser & Photonics Reviews **10**, 1009–1015 (2016).

[30] Marco P. Fischer, Christian Schmidt, Emilie Sakat, Johannes Stock, Antonio Samarelli, Jacopo Frigerio, Michele Ortolani, Douglas J. Paul, Giovanni Isella, Alfred Leitenstorfer, Paolo Biagioni, and Daniele Brida, Optical activation of germanium plasmonic antennas in the mid-infrared, Phys. Rev. Lett. **117**, 047401 (2016).

[31] Stefano Palomba and Lukas Novotny, Nonlinear Excitation of Surface Plasmon Polaritons by Four-Wave Mixing, Physical Review Letters **101**, 056802 (2008).

[32] Yongmin Liu, Stefano Palomba, Yongshik Park, Thomas Zentgraf, Xiaobo Yin, and Xiang Zhang, Compact Magnetic Antennas for Directional Excitation of Surface Plasmons, Nano Letters **12**, 4853–4858 (2012).

[33] J. Lin, J. P. B. Mueller, Q. Wang, G. Yuan, N. Antoniou, X.-C. Yuan, and F. Capasso, Polarization-Controlled Tunable Directional Coupling of Surface Plasmon Polaritons, Science **340**, 331–334 (2013).

[34] Anders Pors, Michael G. Nielsen, Thomas Bernardin, Jean-Claude Weeber, and Sergey I. Bozhevolnyi, Efficient unidirectional polarization-controlled excitation of surface plasmon polaritons, Light: Science & Applications **3**, e197 (2014).

[35] Yimu Bao, Hao Liang, Huimin Liao, Zhi Li, Chengwei Sun, Jianjun Chen, and Qihuang Gong, Efficient Unidirectional Launching of Surface Plasmons by Multi-Groove Structures, Plasmonics **12**, 1425–1430 (2017).

[36] V. S. C. Manga Rao and S. Hughes, Single quantum-dot purcell factor and β factor in a photonic crystal waveguide, Physical Review B **75**, 205437 (2007).

[37] D. E. Aspnes and A. A. Studna, Dielectric functions and optical parameters of Si, Ge, GaP, GaAs, GaSb, InP, InAs, and InSb from 1.5 to 6.0 eV, Physical Review B **27**, 985–1009 (1983).

[38] A Femius Koenderink, Plasmon Nanoparticle Array Waveguides for Single Photon and Single Plasmon Sources, Nano Letters **9**, 4228–4233 (2009).

[39] A. Alú and N. Engheta, Theory of linear chains of metamaterial/plasmonic particles as sub-diffraction optical nanotransmission lines, Physical Review B **74**, 205436 (2006).

[40] C F Bohren and D R Huffman, *Absorption and scattering of light by small particles* (New York: Wiley, 1998).

[41] Roman S. Savelev, Alexey P. Slobozhanyuk, Andrey E. Miroshnichenko, Yuri S. Kivshar, and Pavel A. Belov, Subwavelength waveguides composed of dielectric nanoparticles, Physical Review B **89**, 035435 (2014).

[42] L Novotny and B Hecht, *Principles of Nano-Optics* (Cambridge University Press, 2006).

[43] P. Yu and M. Cardona, *Fundamentals of semiconductors* (Springer, 2005).

[44] C. V. Shank, R. Yen, and C. Hirlimann, Time-resolved reflectivity measurements of femtosecond-optical-pulse-induced phase transitions in silicon, Phys. Rev. Lett. **50**, 454 (1983).

[45] Thibault J.Y. Derrien, Tatiana E. Itina, Rémi Torres, Thierry Sarnet, and Marc Sentis, Possible surface plasmon polariton excitation under femtosecond laser irradiation of silicon, Journal of Applied Physics **114**, 083104 (2013).

[46] See Supplemental Material at [URL] for spectral dependences of the Purcell factor for different emitter locations in orthogonal direction.

[47] Manuel Peter, Andre Hildebrandt, Christian Schlickriede, Kimia Gharib, Thomas Zentgraf, Jens Förstner, and Stefan Linden, Directional Emission from Dielectric Leaky-Wave Nanoantennas, Nano Letters **17**, 4178–4183 (2017).

[48] Alexander E. Krasnok, Alex Maloshtan, Dmitry N. Chigrin, Yuri S. Kivshar, and Pavel A. Belov, Enhanced emission extraction and selective excitation of NV centers with all-dielectric nanoantennas, Laser & Photonics Reviews **9**, 385–391 (2015).

[49] Alexander E Krasnok, Alexey P Slobozhanyuk, Constantin R Simovski, Sergei A Tretyakov, Alexander N Poddubny, Andrey E Miroshnichenko, Yuri S Kivshar, and Pavel A Belov, An antenna model for the purcell effect, Scientific Reports **5**, 12956 (2015).

[50] J. M. Liu, Simple technique for measurements of pulsed Gaussian-beam spot sizes, Optics Letters **7**, 196 (1982).

[51] Sergey V. Makarov, Valentin A. Milichko, Ivan S. Mukhin, Ivan I. Shishkin, Dmitry A. Zuev, Alexey M. Mozharov, Alexander E. Krasnok, and Pavel A. Belov, Controllable femtosecond laser-induced dewetting for plasmonic applications, Laser & Photonics Reviews **10**, 91–99 (2016).

[52] Linhan Lin, Jianli Zhang, Xiaolei Peng, Zilong Wu, Anna C. H. Coughlan, Zhangming Mao, Michael A. Bevan, and Yuebing Zheng, Opto-thermophoretic assembly of colloidal matter, Science Advances **3**, e1700458 (2017).

[53] See Supplemental Material at [URL] for the nanoantenna design based on cylindrical Si particles.

[54] D. H. Reitze, T. R. Zhang, W. M. Wood, and M. C. Downer, Two-photon spectroscopy of silicon using femtosecond pulses at above-gap frequencies, J. Opt. Soc. Am. B **7**, 84 (1990).

[55] G. A. Wurtz, R. Pollard, W. Hendren, G. P. Wiederrecht, D. J. Gosztola, V. A. Podolskiy, and A. V. Zayats, Designed ultrafast optical nonlinearity in a plasmonic nanorod metamaterial enhanced by nonlocality, Nature Nanotechnology **6**, 107–111 (2011).

[56] Ventsislav K. Valev, Denitza Denkova, Xuezhi Zheng, Arseniy I. Kuznetsov, Carsten Reinhardt, Boris N. Chichkov, Gichka Tsutsumanova, Edward J. Osley, Veselin Petkov, Ben De Clercq, Alejandro V. Silhanek, Yogesh Jeyaram, Vladimir Volskiy, Paul A. Warburton, Guy A. E. Vandenbosch, Stoyan Russev, Oleg A. Aktsipetrov, Marcel Ameloot, Victor V. Moshchalkov, and Thierry Verbiest, Plasmon-Enhanced Sub-Wavelength Laser Ablation: Plasmonic Nanojets, Advanced Materials **24**, OP29–OP35 (2012).

[57] Dmitry A Zuev, Sergey V Makarov, Ivan S Mukhin, Valentin A Milichko, Sergey V Starikov, Ivan A Morozov, Ivan I Shishkin, Alexander E Krasnok, and Pavel A Belov, Fabrication of hybrid nanostructures via nanoscale laser-induced reshaping for advanced light manipulation, Advanced Materials **28**, 3087–3093 (2016).

[58] Yuanmu Yang, Wenyi Wang, Abdelaziz Boulesbaa, Ivan I. Kravchenko, Dayrl P. Briggs, Alexander Puretzky, David Geohegan, and Jason Valentine, Nonlinear Fano-Resonant Dielectric Metasurfaces, Nano Letters **15**, 7388–7393 (2015).